

Article

Tetracycline Removal by Activating Persulfate with Diatomite Loading of Fe and Ce

Chongning Lv¹, Jindou Shi², Qiuju Tang² and Qi Hu^{2,*}

¹ School of Traditional Chinese Materia Medica, Shenyang Pharmaceutical University, Shenyang 110016, China; lcnmi@syphu.edu.cn

² School of Pharmaceutical Engineering, Shenyang Pharmaceutical University, Shenyang 110016, China; shijindou1996@foxmail.com (J.S.); tangqiuju96@foxmail.com (Q.T.)

* Correspondence: huqi@syphu.edu.cn; Tel.: +86-24-43520205

Received: 28 October 2020; Accepted: 24 November 2020; Published: 25 November 2020



Abstract: Persulfate (PS)-based oxidation technology is efficient in removing refractory organics from water. A novel diatomite (DIA) support Fe and Ce composite (Fe-Ce/DIA) was prepared for activating persulfate to degrade tetracycline in water. The Fe and Ce were uniformly loaded on DIA, and the total pore size of Fe-Ce/DIA was $6.99 \times 10^{-2} \text{ cm}^3/\text{g}$, and the average pore size was 12.06 nm. Fe-Ce/DIA presented a good catalytic activity and 80% tetracycline was removed under the persulfate system. The Fe-Ce/DIA also had photocatalytic activity, and the corresponding tetracycline removal efficiency was 86% under UV irradiation. Fe-Ce/DIA exhibited less iron dissolution rate compared with Fe-DIA. The tetracycline degradation rate was enhanced when the temperature increased. The optimal tetracycline removal efficiency was obtained when the conditions were of persulfate 10 mM, Fe-Ce/DIA dosage 0.02 g/L, and tetracycline concentration 50 mg/L. In addition, Fe-Ce/DIA showed a wide pH application and good reusability and stability.

Keywords: tetracycline; persulfate; advance oxidation; diatomite; wastewater

1. Introduction

Nowadays, the global pharmaceutical industry develops rapidly, and hundreds of antibiotics have been discovered and applied in human and animal medicine. China consumed 1.62×10^5 tonnes of antibiotics in 2013, and approximately 52% of the antibiotics were used in livestock breeding and aquaculture [1], and the total production increased to 1.96×10^5 tonnes in 2019. Whenever antibiotics are used, wastes with residual antibiotics are inevitable and eventually discharged into the water environment. The concentration of antibiotics in surface water was 10, 15, 50, and 450 $\mu\text{g}/\text{L}$ in Europe, the United States, Africa, and the Asia Pacific [2], which may endanger the quality of the aquatic ecological environment [3,4]. Tetracycline (Figure S1), as a representative antibiotic, is widely used in animal production worldwide [5]. China is the biggest supplier of the Active Pharmaceutical Ingredient (API) of tetracycline. The abuse of tetracycline had caused the universal presence of its residuals and metabolites in environments, in particular, these antibiotics are detected by the Wastewater Treatment Plants (WWTPs) [6–9]. Antibiotics, even in little concentrations, could become a serious threat to ecological security. Thus, effective antibiotic removal approaches should be explored.

Numerous approaches have been employed to remove antibiotics from wastewaters, including biodegradation [10], coagulation/flocculation [11], adsorption [12,13], membrane separation [14], and advanced oxidation processes (AOP) [15–18]. However, biodegradation methods have difficulty in obtaining suitable microorganisms from those that survive in antibiotics [19,20]; adsorption and membrane methods only accumulate and transfer antibiotics from one to another [21–24]. Compared with the above, advanced oxidation processes (AOP) can degrade antibiotics by the

production of reactive free radicals, such as hydroxyl radical (HO^\bullet) or sulfate radical ($\text{SO}_4^{\bullet-}$) [25,26]. Fenton is a common AOP process, and H_2O_2 is catalyzed by Fe^{2+} to produce HO^\bullet for degrading organic pollutants into small molecules such as CO_2 , H_2O and inorganic salts in the process. However, Fenton is limited by the narrow pH-scale [27,28]. As a Fenton-like reagent, persulfate can be used as the oxidizing agent to produce $\text{SO}_4^{\bullet-}$ to degrade organics in water [29]. $\text{SO}_4^{\bullet-}$ has get increasing attention because of its wider pH range [30], longer half-time, and stronger oxidation selectivity in wastewater treatment [31]. The cost for chemicals and reactors was approximately 0.15–0.75 \$/tonne. $\text{SO}_4^{\bullet-}$ can be formed by persulfate and several activators, such as UV-light, heat, base, and electrode transition metal ions [32,33].

Fe is a cheap and abundant crust mineral that is commonly used as a catalyst [34]. The advantages of Fe-based catalysts are as follows: Rich in the earth, easy to produce, and nearly non-toxic [35]. Xu et al. [36] used ferrous ion activating PS to degrade dye orange G, and the decolorization rate of orange G reached 99%. However, the Fe^{3+} , formed by the oxidation of Fe^{2+} , was easily precipitated into iron mud. The serious iron ion dissolution condition restricts the large-scale application of iron-based catalysts. Therefore, some studies attempted to improve the activity and stability of the catalysts, such as, (1) introduce other metal to improve the catalytic activity; (2) provide a supporter for the catalyst to change the physical structure of the catalyst. Among many metal elements, rare earth is widely used in heterogeneous catalysis for its special redox properties. Cerium (Ce) is one of the most abundant rare earth elements. As a dispersant and stabilizer, it was used to strengthen adsorption and catalytic oxidation effects. The cycle from Ce^{3+} to Ce^{4+} makes CeO_2 have good electron transfer characteristics and catalytic oxidation activity. The doping of CeO_2 can improve the storage and activity of lattice oxygen. Perez-Alonso and coworkers reported that the cerium link with iron could increase the performance of catalysts and reduce the dissolution rate of iron [37].

Metal catalysts tend to agglomerate [38,39], and a carrier can help prevent agglomeration [40]. In terms of Fe-based catalysts carrier selection, the current research focuses on new functional materials, such as metal-organic frameworks, carbon nanotubes, graphene oxide, etc., but the complex preparation process and the high price of these materials cause a cost inefficiency. Diatomite (DIA) is porous and cheap, and has strong adsorption capacity [41] and stable chemical properties [42,43]. Some studies used DIA as a carrier: V-doped TiO_2/DIA showed excellent performance as a photocatalyst for degrading rhodamine [44]; $\text{Cu}_2\text{O-ZnO}/\text{DIA}$ showed good performance in degrading red water [45]; Ce-doped TiO_2/DIA granular composite could enhance photocatalytic activity [46]. As is seen from the above, DIA is a potential Fe-based catalysts carrier.

To combine the advantages of Fe/Ce and DIA, a series of DIA matrix composites (Fe-DIA, Ce-DIA, Fe-Ce/DIA) were fabricated to activate persulfate to degrade tetracycline in water. The composites were characterized to show the combination of Fe and Ce. The adsorptive and catalytic ability of DIA containing Fe and Ce was compared through tetracycline removal. The iron dissolution and reusability of the Fe-Ce/DIA were measured. Finally, the parameters for tetracycline removal were given through investigating the Fe-Ce/DIA dosage, tetracycline initial concentration, pH, and temperature in the reaction.

2. Results

2.1. Characterization of the Composites

Specific surface areas of the DIA and Fe-Ce/DIA, as determined by the Brunauer–Emmett–Teller (BET) method using N_2 adsorption-desorption curves, were found to be 40.11 m^2/g and 21.04 m^2/g , respectively. The total pore size of DIA and Fe-Ce/DIA was 9.67×10^{-2} and 6.99×10^{-2} cm^3/g , and the corresponding average pore size was 9.64 and 12.06 nm (Figure 1), respectively. The surface area and total pore volume decreased with the load of Fe and Ce, but the average pore diameter increased in the process. Some microspores in DIA were blocked by the carried metal and larger diameter holes remained in the process, which decreased the total pore size and increased the average pore diameter.

The change might be beneficial for pollutants adsorption based on the previous report [47]. The SEM image indicated that the surface of Fe-Ce/DIA was more compact and the pores were less clear than that of DIA (Figure 2).

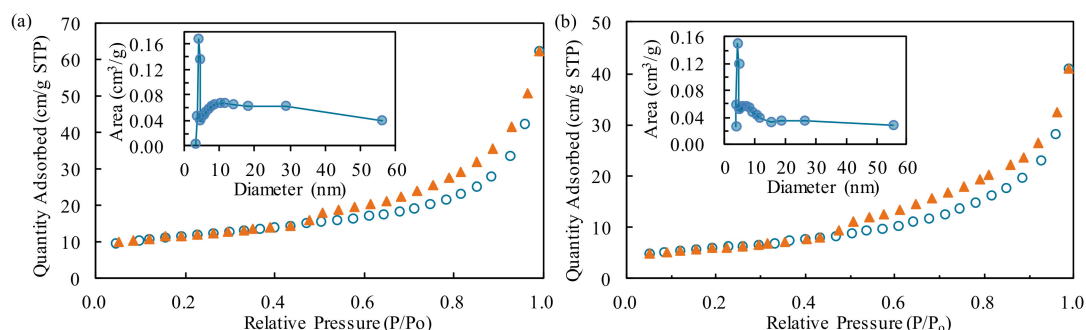


Figure 1. N₂ adsorption-desorption isotherms of diatomite (DIA) (a) Fe-Ce/DIA (b); inset: The pore size distribution.

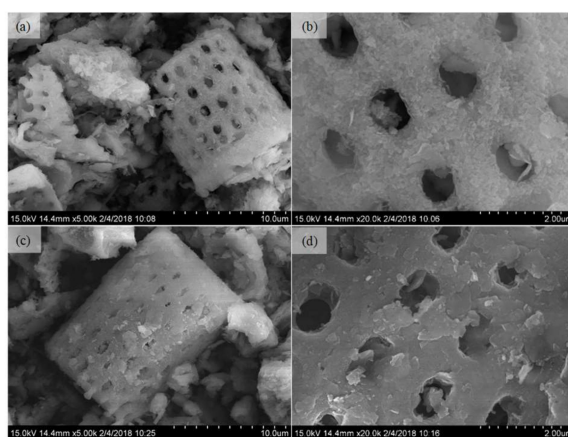


Figure 2. SEM images of DIA (a,b) and Fe-Ce/DIA (c,d).

To clearly show the microstructure of DIA and Fe-Ce/DIA, Transmission Electron Microscope (TEM) was used to detect the samples (Figure 3). Fe-Ce/DIA was more compact than DIA from TEM photos at 200 nm (Figure 3a,b). At 50 nm, some dark and light areas were shown (Figure 3c): The dark part was Fe₃O₄ and the light was CeO₂, and both Fe and Ce were dispersed into the framework of Fe-Ce/DIA. High-resolution TEM image showed that lattice fringes of CeO₂ displayed interplanar spacings in the particles (Figure 3d).

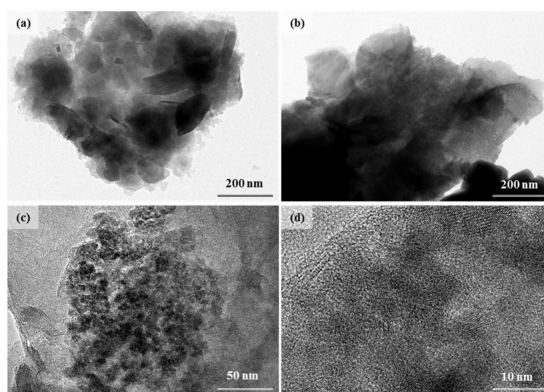


Figure 3. TEM images of DIA (a) and Fe-Ce/DIA (b-d).

Figure 4 depicted the XRD pattern of Fe-Ce/DIA, the diffraction peaks appearing at 36.82° , 55.62° , and 59.30° were attributed to the (311), (422), and (511) diffractive surfaces of the Fe_3O_4 apical crystal (Fm-3 m (227), JCPDS no.74-0748), respectively. The peaks at 21.14° , 27.33° , and 51.69° represented (110), (112), and (304) diffractive surfaces of the CeO_2 fluorite (Fm-3 m (225), JCPDS no. 34-0394), which indicated that Fe and Ce were successfully loaded on diatomite.

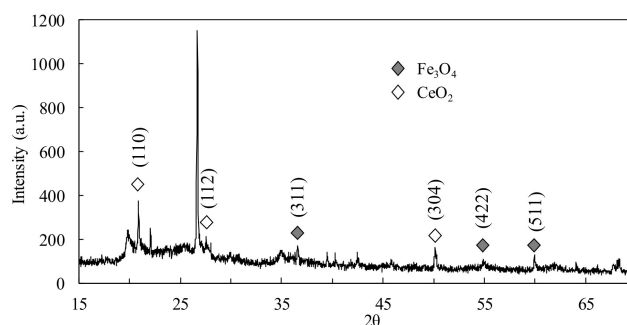


Figure 4. XRD patterns of Fe-Ce/DIA.

2.2. The Adsorptive and Catalytic Properties

The tetracycline adsorption by DIA, Fe-Ce/DIA, Fe-DIA, and Ce-DIA was compared under the same conditions (Figure 5). The tetracycline removal by DIA adsorption was about 20% under the dark. The combination of Fe, Ce and DIA could increase the adsorption capacity, and the best efficiency was 30% for Fe-Ce/DIA. The doping of Fe and Ce provided a rough surface, which probably improved the adsorption capacity of Fe-Ce/DIA.

The tetracycline degradation by DIA, Fe-Ce/DIA, Fe-DIA, and Ce-DIA was also investigated through adding persulfate. The load of Fe or Ce could improve the catalytic activity, the removal efficiency by Ce-DIA was about 70%, while that of Fe-DIA and Fe-Ce/DIA were 80% (Figure 5b). The result indicated that Fe-Ce/DIA and Fe-DIA effectively activated persulfate to degrade tetracycline. The Fe-Ce/DIA and Fe-DIA had the same catalytic efficiency in the same dosage, but Fe content in Fe-Ce/DIA was less, which means less iron dissolution.

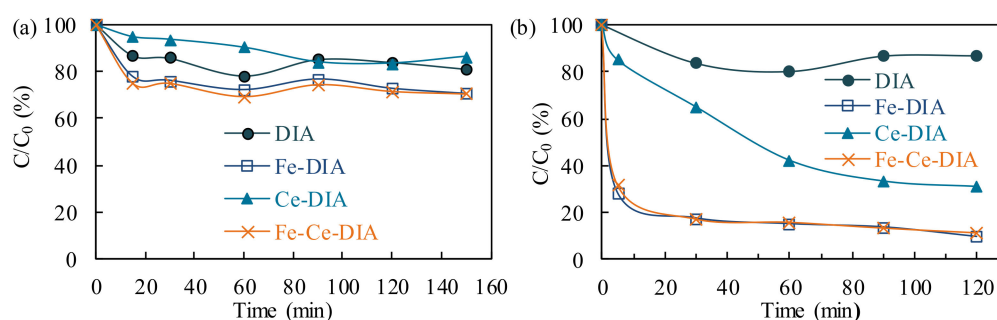


Figure 5. Tetracycline adsorption by DIA, Fe-DIA, Ce-DIA, and Fe-Ce/DIA (a); tetracycline degradation by adding persulfate (b). Conditions: (Tetracycline) = 200 mL, 50 mg/L, (Catalyst) = 0.02 g, (Persulfate) = 0.134 g, $T = 37^\circ\text{C}$, 150 rpm.

2.3. Photocatalytic Property

The photocatalytic activity of Fe-Ce/DIA was investigated under visible and ultraviolet light. The tetracycline removal by Fe-DIA was slightly better than Fe-Ce/DIA, as Fe-DIA contained more Fe in the same dosage (Figure 6a). The final removal rates were 86% (Fe-Ce/DIA) and 91% (Fe-DIA). Besides, CeO_2 had a strong absorption in the ultraviolet region, and some photogenerated electron pair holes were produced and reacted with water to produce hydroxyl radicals [48,49]. Thus, Fe-Ce/DIA showed better photocatalytic properties than Fe-DIA during the first 20 min (Figure 6b). CeO_2 exhibited poor

photocatalytic activity under visible light, but showed good activity under ultraviolet light (Figure 6). CeO_2 had a wide band gap of 3.2 eV and only absorbed light with a wavelength less than 444 nm, which led to its little absorption under visible light and thus poor catalytic activity [48].

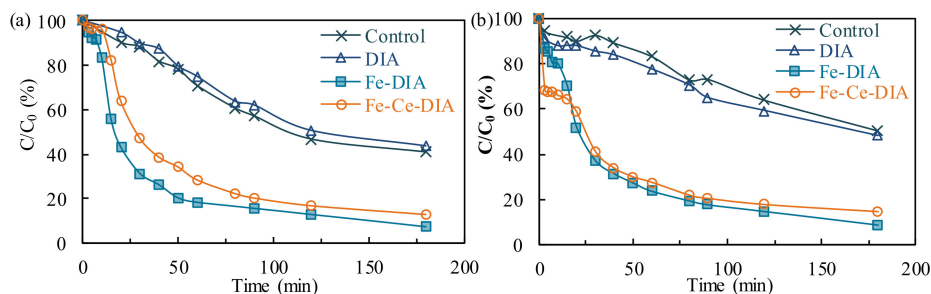


Figure 6. The photocatalytic effect under different light condition: Visible light (a); ultraviolet light (b).

2.4. Metal Leaching and the Reusability of Fe-Ce/DIA

The dissolved Fe in the catalytic process was detected to show the metal leaching (Figure 7). Dissolved Fe increased rapidly in the first 90 min and then trended to be stable for Fe-DIA, by contrast, the dissolved Fe increased slowly for Fe-Ce/DIA in the process. Ce inhibited the loss of Fe^{2+} and improved the stability of the Fe-Ce/DIA.

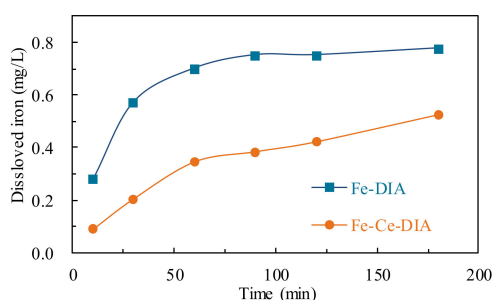


Figure 7. Determination of dissolved Fe in the tetracycline solution.

Reusability is an important factor to evaluate the cost-effectiveness of a catalyst. At the same condition, the tetracycline removal efficiency of Fe-Ce/DIA was better than that of Fe-DIA. Fe-DIA lost the active component (Fe^{2+}) and less SO_4^- was produced during the recycles (Figure 8). After 3 times, Fe-Ce/DIA still showed good catalytic performance.

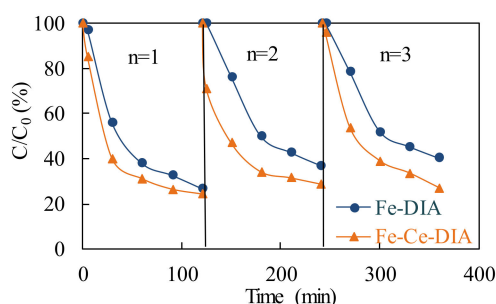


Figure 8. Repeated use of Fe-DIA and Fe-Ce/DIA for TC removal. Conditions: $T = 37^\circ\text{C}$, 150 rpm.

2.5. Parameters on Tetracycline Removal by Fe-Ce/DIA

The effect of Fe-Ce/DIA dosage on the tetracycline removal was investigated at five different dosages. Fe^{2+} was a necessary catalyst for sodium persulfate to generate free radicals. At the same

reaction time, higher removal efficiencies were obtained with the dosage from 0 to 0.01 g/L, the reaction rate increased from $2.4 \times 10^{-3} \text{ min}^{-1}$ to $8.6 \times 10^{-3} \text{ min}^{-1}$. When the dosage of Fe-Ce/DIA was 0.02 g/L, the reaction rate decreased to $6.1 \times 10^{-3} \text{ min}^{-1}$ (Figure 9, Table 1). The similar result had been obtained in organic pollutants degradation by activated persulfate [50]. The decline can be explained as follows: Due to the aggregation of excessive catalyst, reactants cannot enter the active center; Fe is consumed by SO_4^- if it exceeds a certain amount as Equation (1) [50]. The optimum dosage of Fe-Ce/DIA was 0.01 g/L in this study. Therefore, considering the cost and efficiency of tetracycline removal, a dosage of 0.01 g/L Fe-Ce/DIA was selected for the successive tetracycline removal study.

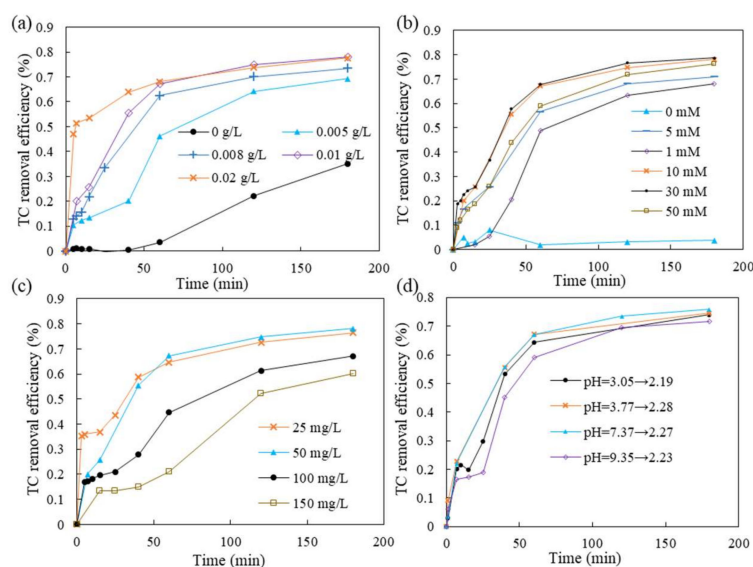


Figure 9. The effects of catalyst dosage (a); persulfate dosage (b); tetracycline concentration (c); pH (d) on Tetracycline (TC) removal. Conditions: (Tetracycline) = 200 mL, 50 mg/L, (Catalyst) = 0.02 g, (Persulfate) = 0.476 g, T = 30 °C, 150 rpm.

Table 1. The reaction rate of tetracycline degradation at different dosages of Fe-Ce/DIA.

Dosage of Fe-Ce/DIA (g/L)	Reaction Rate Constant k (min^{-1})	R^2
0	2.4×10^{-3}	0.9928
0.005	6.9×10^{-3}	0.9468
0.008	7.5×10^{-3}	0.8700
0.010	8.3×10^{-3}	0.8473
0.020	6.1×10^{-3}	0.7022

The dosage of sodium persulfate was an important parameter on tetracycline removal. A higher reaction rate was obtained with a higher sodium persulfate dosage from 1 to 30 mM, but the reaction rate decreased when the dosage of sodium persulfate exceeded 30 mM (Figure 9, Table 2). This phenomenon can be explained by the increase of SO_4^- , which is obtained from the increasing dosage of sodium persulfate. Moreover, the collision probability between SO_4^- and tetracycline was increased, and the combined action of the two accelerated the reaction rate, so the reaction rate constantly increased. However, when the dosage of sodium persulfate was increased to a certain extent, as the interaction between SO_4^- and $\text{S}_2\text{O}_8^{2-}$, SO_4^- would react with $\text{S}_2\text{O}_8^{2-}$ to form SO_4^{2-} and

$S_2O_8^{\cdot-}$ (Equations (2) and (3)). Besides, $SO_4^{\cdot-}$ may inhibit the formation of HO^{\bullet} . In this study, 10 mm was selected as a proper dosage for tetracycline removal.

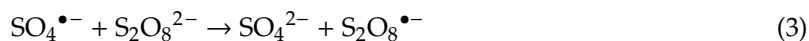


Table 2. The reaction rate of tetracycline degradation at different dosages of persulfate.

Dosage of PS (mM)	Reaction Rate Constant k (min^{-1})	R^2
0	0.6×10^{-4}	0.0782
1	6.7×10^{-3}	0.9080
5	7.1×10^{-3}	0.9061
10	8.3×10^{-3}	0.9094
30	8.5×10^{-3}	0.9016
50	8.2×10^{-3}	0.9203

The effect of the initial tetracycline concentrations on tetracycline removal was also investigated. The removal efficiency decreased with an increase in initial concentrations (Figure 9c, Table 3). As the number of producing free radicals was maintained the same, the increase in initial tetracycline concentration led to the reduction of tetracycline oxidized by $SO_4^{\cdot-}$ per unit volume in unit time.

Table 3. The reaction rate of tetracycline degradation at different initial concentrations.

Concentration of TC (mg/L)	Reaction Rate Constant k (min^{-1})	R^2
25	9.2×10^{-3}	0.8321
50	8.3×10^{-3}	0.8473
100	6.0×10^{-3}	0.006
150	5.3×10^{-3}	0.0053

The initial pH was an important parameter on tetracycline removal because it can affect the activation of persulfate and the existent forms of tetracycline (Figure 9d, Table 4). Tetracycline had four forms under different pH conditions (H_3TC^+ , H_2TC , HTC^- , and TC^{2-}). Fe^{2+} was stable in acid condition and produced more $SO_4^{\cdot-}$, but in the alkaline condition, $SO_4^{\cdot-}$ could be converted into HO^{\bullet} , and $SO_4^{\cdot-}$ was quenched by the increasing HO^{\bullet} . The results were presented in the Figure 9d and Table 4. It could be observed that the reaction rate was the same under different pH conditions, consistent with Zhao et al. [51]. The decrease of pH value may be due to the small organic acid molecules and HSO_4^- produced in the reaction process. The final pH of the reactions was 2.19–2.33, which were in the same range.

Table 4. The reaction rate of tetracycline degradation at different pH.

pH of Solution	Reaction Rate Constant k (min^{-1})	R^2
3.05	7.4×10^{-3}	0.8089
3.77	7.3×10^{-3}	0.7661
7.34	8.0×10^{-3}	0.8179
9.53	7.5×10^{-3}	0.8780

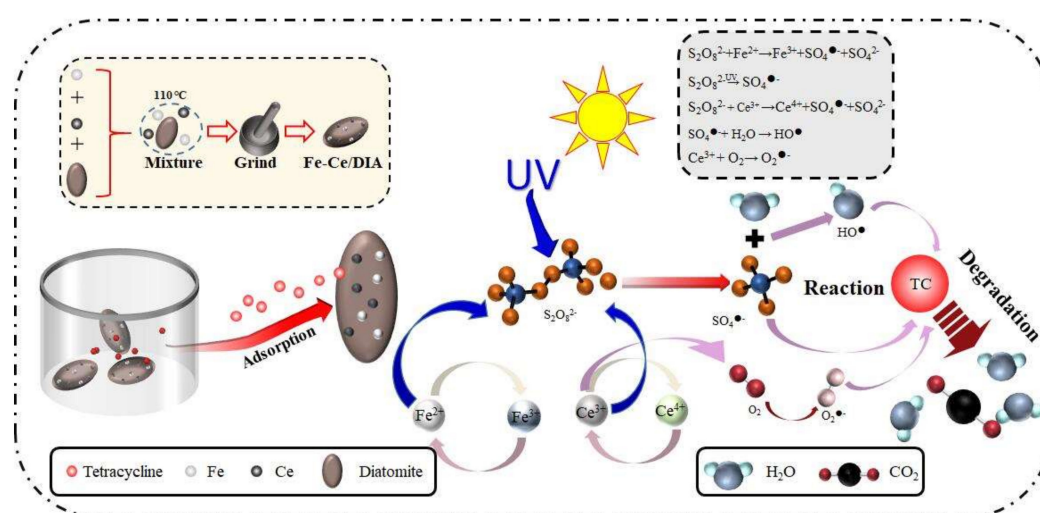
The effect of temperature on tetracycline removal was evaluated at 25, 30, 35, and 40 °C. The tetracycline removal efficiency increased with the temperature increasing (Table 5). As more energy was absorbed in higher temperatures, the O-O bond in sodium persulfate was more likely to break, resulting in more $SO_4^{\cdot-}$.

Table 5. The reaction rate of tetracycline degradation at different temperatures.

T (°C)	Reaction Rate (min ⁻¹)	R ²
25	1.81×10^{-2}	0.9194
30	1.83×10^{-2}	0.9920
35	1.86×10^{-2}	0.9686
40	1.98×10^{-2}	0.9524

2.6. Degradation Mechanism

Fe-Ce/DIA showed good performance on tetracycline removal, and a potential removal mechanism was proposed as shown in Figure 10. Firstly, Tetracycline and persulfate were absorbed on the surface of Fe-Ce/DIA. Tetracycline antibiotics were positively charged in acidic solutions and anionic under alkaline conditions [52]. DIA was negatively charged at most pH conditions. In acid condition, tetracycline adsorption by diatomite depended on positive and negative charge; in alkaline condition, tetracycline was adsorbed by cation on diatomite. Fe²⁺ could activate persulfate to produce SO₄^{•-}. Ce³⁺ can also activate persulfate to produce SO₄^{•-} [28]. The persulfate could be activated by ultraviolet light [8,53]: SO₄^{•-} reacted with H₂O to form HO[•] radicals, and Ce³⁺ activated O₂ to produce O₂^{•-}. Finally, tetracycline was degraded into H₂O and CO₂ by all active radicals (HO[•], SO₄^{•-} and O₂^{•-}). Eight main products were found in the degradation process, and the degradation products included m/z 475, 459, 443, 430, 441, 414, 386, and 342. The detail results were shown in Table S1 and Figure S2.

**Figure 10.** Potential mechanism of activation of persulfate by Fe-Ce/DIA to degrade tetracycline.

3. Materials and Methods

3.1. Chemicals

Diatomite (DIA, CP) was purchased from Ruijinte Chemical Co., Ltd. (Tianjin, China). Barium nitrate hexahydrate (Ce(NO₃)₂·6H₂O) was procured from Guangfu Fine Chemical Research Institute (Tianjin). FeSO₄, NH₃·H₂O, and NaOH were acquired from Damao Chemical Reagent Factory (Tianjin). Sodium chloride, methanol and sulfuric acid were obtained from Keanlong Bohua Pharmaceutical Chemical Co., Ltd. (Tianjin). Citric acid, sodium sulfate, ammonium ferrous sulfate, and hydroxylamine hydrochloride were acquired from Bodi Chemical Co., Ltd. (Tianjin, China). 1, 10-Phenanthroline was purchased from Sinopharm Chemical Reagent Co., Ltd. (Shanghai, China). All chemicals were of analytical grade.

3.2. Synthesis of Composites

DIA (3 g) was calcined at 300 °C for 2 h, mixed with NaCl solution, stirred in a water bath at 65 °C for 2 h, washed until no Cl⁻ detection, and dried at 110 °C. The solid-liquid ratio of DIA and NaCl (60 mL 1.0 mol/L) was 1:20.

Ce(NO₃)₂·6H₂O (0.043 g) was dissolved in water (50 mL) and mixed with FeSO₄ (1.043 g). The total concentration of Fe²⁺ and Ce²⁺ was 0.1 mol/L. The solution was mixed with dried DIA, added with citric acid (1.051 g) and stirred in a water bath (60 °C for 2 h, 80 °C for 1 h). Ammonia water was added during the reaction to maintain the precursor pH = 8.0. The material was dried at 110 °C, calcined at 400 °C for 2 h, and ground to obtain Fe-Ce/DIA. The Fe-DIA and Ce-DIA were also synthesized by the same method as Fe-Ce/DIA.

3.3. Characterization of Composites

X-ray diffractometer (XRD, Bruker D8 Advance, Karlsruhe, Germany) was used to test the crystal properties. Scanning electron microscopy (SEM, JEM1002EX) was used to analyze microscopic morphology and element distribution. The pore structure and specific surface area characteristics of the composites were tested using a physical adsorption instrument (BET, ASAP 2460, Micrometrics, Norcross, GA, USA).

3.4. Adsorption Study

The adsorption capacity of Fe-Ce/DIA, Fe-DIA, Ce-DIA, and DIA to tetracycline was investigated before a degradation study. Each sample (0.020 g) was dissolved in tetracycline (200 mL, 50 mg/L) separately, then reacted in dark for 2.5 h (37 °C, 150 rpm). The sample (3 mL, reacted for 0, 30, 60, 90, 120, and 180 min) was filtered using a 0.22 µm filter, extracted in EP tube for 2 mL, mixed with CH₃OH (3 mL), and measured for absorbance at 359 nm. The basic calculations in adsorption can be found in previous study [32,54].

3.5. Degradation Study

The tetracycline degradation by Fe-Ce/DIA, Fe-DIA, Ce-DIA, and DIA was investigated. Each sample (0.02 g) was dissolved in tetracycline (200 mL, 50 mg/L), added with sodium persulfate (0.134 g) to react in dark for 2 h (37 °C, 150 rpm). The samples (3 mL, reacted for 0, 30, 60, 90, and 120 min) were processed and measured as described above.

The effect of visible light and ultraviolet on tetracycline degradation were investigated. Each sample (0.02 g), Fe-Ce/DIA, Fe-DIA, Ce-DIA, and DIA, was dissolved in tetracycline (200 mL, 50 mg/L) separately, and then sodium persulfate (0.426 g) was added to the system. The reaction was under Xe lamp (25 A, 500 W) and Hg lamp (5.2 A, 350 W) with magnetic stirring at 650 rpm.

A UPLC system coupled with a Bruker's Compact high-resolution time-of-flight (TOF) mass spectrometer was applied to the UPLC-MS/MS analysis of samples to identify the structure of the degradation products of tetracycline.

Chromatographic separation was achieved using an C18 column (2.1 mm × 100 mm, 1.7 µm). The column temperature was maintained at 30 °C, and the mobile phase, at a flow rate of 0.2 mL/min, consisted of solvent A (0.1% acetic acid in water) and mobile phase B (methanol). The gradient program of the mobile phase was as follows: 0–20 min, 15–55% B. Mass spectrometry conditions: Electrospray interface (ESI), MS analysis in negative ion mode, mass-nucleus ratio scan range 100–800, collision energy is 12 eV.

3.6. Batch Study of Tetracycline Removal

The effect of the various parameters, including the dosage of composites (Fe-Ce/DIA, Fe-DIA, Ce-DIA, and DIA) and sodium persulfate, initial pH and tetracycline concentrations, were investigated in details. The reusability of the composites (Fe-Ce/DIA and Fe-DIA) were performed by placing

0.002 g Fe-Ce/DIA or Fe-DIA in 200 mL of 50 mg/L tetracycline solution and adding sodium persulfate of 0.476 g, respectively.

4. Conclusions

A series of composites (Fe-Ce/DIA, Fe-DIA, Ce-DIA) were synthesized to remove tetracycline from water. The average pore size of Fe-Ce/DIA was larger than DIA, which was beneficial to tetracycline adsorption. SEM and TEM images showed Fe and Ce were uniformly dispersed in DIA. The tetracycline removal efficiency was 80% at the catalytic oxidation system provided by Fe-Ce/DIA and persulfate. Ultraviolet light could promote the removal efficiency, and 86% tetracycline was removed by Fe-Ce/DIA activating persulfate under ultraviolet light. Eight main products were found in the tetracycline degradation process. A recommended parameter was of Fe-Ce/DIA dosage 0.02 g, persulfate 10 mM, and initial tetracycline solution 50 mg/L. The iron dissolution of Fe-Ce/DIA was less than Fe-DIA in activating persulfate. Fe-Ce/DIA showed wide pH application and excellent reusability in tetracycline removal. The metal doped diatomite is a promising catalyst in antibiotics pollution control.

Supplementary Materials: The following are available online Table S1: The intermediate products of the tetracycline degradation, Figure S1: The structure of tetracycline, Figure S2: The BPC of intermediate products of the tetracycline degradation.

Author Contributions: Conceptualization, C.L. and Q.H.; methodology, J.S. and Q.T.; visualization, J.S. and Q.T.; validation, C.L. and Q.H.; formal analysis, Q.T.; investigation, C.L., J.S. and Q.T.; resources, Q.H.; data curation, J.S.; writing-original draft preparation, C.L.; supervision, Q.H.; project administration, C.L. and Q.H.; funding acquisition, C.L. and Q.H. All authors have read and agreed to the published version of the manuscript.

Funding: This study was funded by the Young and Middle-aged Key Talent Program of Shenyang Pharmaceutical University (ZQN2018013) and Liaoning Provincial Doctor Startup Fund of China (20180540034).

Conflicts of Interest: The authors declare no conflict of interest.

References

1. Qiao, M.; Ying, G.-G.; Singer, A.C.; Zhu, Y.-G. Review of antibiotic resistance in China and its environment. *Environ. Int.* **2018**, *110*, 160–172. [[CrossRef](#)]
2. Danner, M.-C.; Robertson, A.; Behrends, V.; Reiss, J. Antibiotic pollution in surface fresh waters: Occurrence and effects. *Sci. Total Environ.* **2019**, *664*, 793–804. [[CrossRef](#)] [[PubMed](#)]
3. Li, D.; Yang, M.; Hu, J.; Ren, L.; Zhang, Y.; Li, K. Determination and fate of oxytetracycline and related compounds in oxytetracycline production wastewater and the receiving river. *Environ. Toxicol. Chem.* **2008**, *27*, 80–86. [[CrossRef](#)] [[PubMed](#)]
4. Liu, J.; Wong, M. Pharmaceuticals and personal care products (PPCPs): A review on environmental contamination in China. *Environ. Int.* **2013**, *59*, 208–224. [[CrossRef](#)] [[PubMed](#)]
5. Daghrir, R.; Drogui, P. Tetracycline antibiotics in the environment: A review. *Environ. Chem. Lett.* **2013**, *11*, 209–227. [[CrossRef](#)]
6. Gherghel, A.; Teodosiu, C.; Notarnicola, M.; De Gisi, S. Sustainable design of large wastewater treatment plants considering multi-criteria decision analysis and stakeholders' involvement. *J. Environ. Manag.* **2020**, *261*, 110158. [[CrossRef](#)]
7. Han, Y.; Yang, T.; Xu, G.; Li, L.; Liu, J. Characteristics and interactions of bioaerosol microorganisms from wastewater treatment plants. *J. Hazard. Mater.* **2020**, *391*, 122256. [[CrossRef](#)]
8. Zhou, C.; Wu, J.; Dong, L.; Liu, B.; Xing, D.; Yang, S.; Wu, X.; Wang, Q.; Fan, J.; Feng, L.; et al. Removal of antibiotic resistant bacteria and antibiotic resistance genes in wastewater effluent by UV-activated persulfate. *J. Hazard. Mater.* **2020**, *388*, 122070. [[CrossRef](#)]
9. Talang, R.P.N.; Sirivithayapakorn, S.; Polruang, S. Environmental impacts and cost-effectiveness of Thailand's centralized municipal wastewater treatment plants with different nutrient removal processes. *J. Clean. Prod.* **2020**, *256*, 120433. [[CrossRef](#)]
10. Shao, S.; Hu, Y.; Cheng, J.; Chen, Y. Biodegradation mechanism of tetracycline (TEC) by strain *Klebsiella* sp. SQY5 as revealed through products analysis and genomics. *Ecotox. Environ. Saf.* **2019**, *185*, 109676. [[CrossRef](#)]

11. Xu, Q.; Zhou, Q.; Pan, M.; Dai, L. Interaction between chlortetracycline and calcium-rich biochar: Enhanced removal by adsorption coupled with flocculation. *Chem. Eng. J.* **2020**, *382*, 122705. [[CrossRef](#)]
12. Yao, N.; Li, C.; Yu, J.; Xu, Q.; Wei, S.; Tian, Z.; Yang, Z.; Yang, W.; Shen, J. Insight into adsorption of combined antibiotic-heavy metal contaminants on graphene oxide in water. *Sep. Purif. Technol.* **2020**, *236*, 116278. [[CrossRef](#)]
13. Peng, J.; Wu, E.; Wang, N.; Quan, X.; Sun, M.; Hu, Q. Removal of sulfonamide antibiotics from water by adsorption and persulfate oxidation process. *J. Mol. Liq.* **2019**, *274*, 632–638. [[CrossRef](#)]
14. Guo, Y.-S.; Ji, Y.-L.; Wu, B.; Wang, N.-X.; Yin, M.-J.; An, Q.-F.; Gao, C.-J. High-flux zwitterionic nanofiltration membrane constructed by in-situ introduction method for monovalent salt/antibiotics separation. *J. Membrane Sci.* **2020**, *593*, 117441. [[CrossRef](#)]
15. Chen, Y.; Wu, Q.; Liu, L.; Wang, J.; Song, Y. The fabrication of floating Fe/N co-doped titania/diatomite granule catalyst with enhanced photocatalytic efficiency under visible light irradiation. *Adv. Powder Technol.* **2018**, *30*, 126–135. [[CrossRef](#)]
16. Wammer, K.H.; Lapara, T.M.; Mcneill, K.; Arnold, W.A.; Swackhamer, D.L. Changes in antibacterial activity of triclosan and sulfa drugs due to photochemical transformations. *Environ. Toxicol. Chem.* **2006**, *25*, 1480–1486. [[CrossRef](#)]
17. Rasheed, H.U.; Lv, X.; Zhang, S.; Wei, W.; Nabiullah; Xie, J. Ternary MIL-100(Fe)@Fe₃O₄/CA magnetic nanophotocatalysts (MNPCs): Magnetically separable and Fenton-like degradation of tetracycline hydrochloride. *Adv. Powder Technol.* **2018**, *29*, 3305–3314. [[CrossRef](#)]
18. Sun, Y.; Cho, D.-W.; Graham, N.J.D.; Hou, D.; Yip, A.C.K.; Khan, E.; Song, H.; Li, Y.; Tsang, D.C.W. Degradation of antibiotics by modified vacuum-UV based processes: Mechanistic consequences of H₂O₂ and K₂S₂O₈ in the presence of halide ions. *Sci. Total Environ.* **2019**, *664*, 312–321. [[CrossRef](#)]
19. Jia, A.; Wan, Y.; Xiao, Y.; Hu, J. Occurrence and fate of quinolone and fluoroquinolone antibiotics in a municipal sewage treatment plant. *Water Res.* **2011**, *46*, 387–394. [[CrossRef](#)]
20. Zessel, K.; Mohring, S.; Hamscher, G.; Kietzmann, M.; Stahl, J. Biocompatibility and antibacterial activity of photolytic products of sulfonamides. *Chemosphere* **2014**, *100*, 167–174. [[CrossRef](#)]
21. Ji, L.; Chen, W.; Zheng, S.; Xu, Z.; Zhu, D. Adsorption of sulfonamide antibiotics to multiwalled carbon nanotubes. *Langmuir* **2009**, *25*, 11608–11613. [[CrossRef](#)] [[PubMed](#)]
22. Martucci, A.; Cremonini, M.A.; Blasioli, S.; Gigli, L.; Gatti, G.; Marchese, L.; Braschi, I. Adsorption and reaction of sulfachloropyridazine sulfonamide antibiotic on a high silica mordenite: A structural and spectroscopic combined study. *Micropor. Mesopor. Mater.* **2013**, *170*, 274–286. [[CrossRef](#)]
23. Srinivasan, P.; Sarmah, A.K.; Manley-Harris, M. Co-contaminants and factors affecting the sorption behaviour of two sulfonamides in pasture soils. *Environ. Pollut.* **2013**, *180*, 165–172. [[CrossRef](#)] [[PubMed](#)]
24. Pan, J.; Dong, Z.; Wang, B.; Jiang, Z.; Zhao, C.; Wang, J.; Song, C.; Zheng, Y.; Li, C. The enhancement of photocatalytic hydrogen production via Ti³⁺ self-doping black TiO₂/g-C₃N₄ hollow core-shell nano-heterojunction. *Appl. Catal. B Environ.* **2019**, *242*, 92–99. [[CrossRef](#)]
25. Keen, O.S.; Baik, S.; Linden, K.G.; Aga, D.S.; Love, N.G. Enhanced biodegradation of carbamazepine after UV/H₂O₂ advanced oxidation. *Environ. Sci. Technol.* **2012**, *46*, 6222–6227. [[CrossRef](#)] [[PubMed](#)]
26. Zheng, X.; Xu, S.; Wang, Y.; Sun, X.; Gao, Y.; Gao, B. Enhanced degradation of ciprofloxacin by graphitized mesoporous carbon (GMC)-TiO₂ nanocomposite: Strong synergy of adsorption-photocatalysis and antibiotics degradation mechanism. *J. Colloid Interf. Sci.* **2018**, *527*, 202–213. [[CrossRef](#)]
27. Mousset, E.; Pontvianne, S.; Pons, M.N. Fate of inorganic nitrogen species under homogeneous Fenton combined with electro-oxidation/reduction treatments in synthetic solutions and reclaimed municipal wastewater. *Chemosphere* **2018**, *201*, 6–12. [[CrossRef](#)]
28. Guan, R.; Yuan, X.; Wu, Z.; Jiang, L.; Zhang, J.; Li, Y.; Zeng, G.; Mo, D. Efficient degradation of tetracycline by heterogeneous cobalt oxide/cerium oxide composites mediated with persulfate. *Sep. Purif. Technol.* **2018**, *212*, 223–232. [[CrossRef](#)]
29. Shabanloo, A.; Salari, M.; Shabanloo, N.; Dehghani, M.H.; Pittman, C.U.; Mohan, D. Heterogeneous persulfate activation by nano-sized Mn₃O₄ to degrade furfural from wastewater. *J. Mol. Liq.* **2019**, *298*, 112088. [[CrossRef](#)]
30. Liang, C.; Wang, Z.; Bruell, C.J. Influence of pH on persulfate oxidation of TCE at ambient temperatures. *Chemosphere* **2007**, *66*, 106–113. [[CrossRef](#)]

31. Ao, X.; Sun, W.; Li, S.; Yang, C.; Li, C.; Lu, Z. Degradation of tetracycline by medium pressure UV-activated peroxy monosulfate process: Influencing factors, degradation pathways, and toxicity evaluation. *Chem. Eng. J.* **2018**, *361*, 1053–1062. [[CrossRef](#)]
32. Qu, J.; Meng, X.; Zhang, Y.; Meng, Q.; Tao, Y.; Hu, Q.; Jiang, X.; You, H.; Shoemaker, C.A. A combined system of microwave-functionalized rice husk and poly-aluminium chloride for trace cadmium-contaminated source water purification: Exploration of removal efficiency and mechanism. *J. Hazard. Mater.* **2019**, *379*, 120804. [[CrossRef](#)] [[PubMed](#)]
33. Hu, L.; Zhang, G.; Liu, M.; Wang, Q.; Wang, P. Enhanced degradation of Bisphenol A (BPA) by peroxy monosulfate with $\text{Co}_3\text{O}_4\text{-Bi}_2\text{O}_3$ catalyst activation: Effects of pH, inorganic anions, and water matrix. *Chem. Eng. J.* **2018**, *338*, 300–310. [[CrossRef](#)]
34. Espinosa, J.C.; Catalá, C.; Navalón, S.; Ferrer, B.; Álvaro, M.; García, H. Iron oxide nanoparticles supported on diamond nanoparticles as efficient and stable catalyst for the visible light assisted Fenton reaction. *Appl. Catal. B Environ.* **2018**, *226*, 242–251. [[CrossRef](#)]
35. Wang, J.; Bai, Z. Fe-based catalysts for heterogeneous catalytic ozonation of emerging contaminants in water and wastewater. *Chem. Eng. J.* **2017**, *312*, 79–98. [[CrossRef](#)]
36. Xu, X.-R.; Li, X.-Z. Degradation of azo dye Orange G in aqueous solutions by persulfate with ferrous ion. *Sep. Purif. Technol.* **2010**, *72*, 105–111. [[CrossRef](#)]
37. Abbasi, M.; Mirzaei, A.A.; Atashi, H. Hydrothermal synthesis of Fe-Ni-Ce nano-structure catalyst for Fischer-Tropsch synthesis: Characterization and catalytic performance. *J. Alloys Compd.* **2019**, *799*, 546–555. [[CrossRef](#)]
38. Su, S.; Liu, Y.; He, W.; Tang, X.; Jin, W.; Zhao, Y. A novel graphene oxide-carbon nanotubes anchored $\alpha\text{-FeOOH}$ hybrid activated persulfate system for enhanced degradation of Orange II. *J. Environ. Sci.* **2019**, *83*, 73–84. [[CrossRef](#)]
39. Zhang, G.; Sun, Z.; Duan, Y.; Ma, R.; Zheng, S. Synthesis of nano- TiO_2 /diatomite composite and its photocatalytic degradation of gaseous formaldehyde. *Appl. Surf. Sci.* **2017**, *412*, 105–112. [[CrossRef](#)]
40. Sorolla, M.G., II; Dalida, M.L.; Khemthong, P.; Grisdanurak, N. Photocatalytic degradation of paraquat using nano-sized Cu-TiO_2 /SBA-15 under UV and visible light. *J. Environ. Sci. China* **2012**, *24*, 1125–1132. [[CrossRef](#)]
41. Semião, M.A.; Haminiuk, C.W.I.; Maria, G.M. Residual diatomaceous earth as a potential and cost effective biosorbent of the azo textile dye Reactive Blue 160. *J. Environ. Chem. Eng.* **2020**, *8*, 103617. [[CrossRef](#)]
42. Xu, L.J.; Chu, W.; Gan, L. Environmental application of graphene-based CoFe_2O_4 as an activator of peroxy monosulfate for the degradation of a plasticizer. *Chem. Eng. J.* **2015**, *263*, 435–443. [[CrossRef](#)]
43. Yi, L.M.; Liang, Z.; Liang, L.G.; Fang, N.L.; Chun, S.X. Synthesis and photocatalytic activity of BiOCl /diatomite composite photocatalysts: Natural porous diatomite as photocatalyst support and dominant facets regulator. *Adv. Powder Technol.* **2020**, *31*, 339–350.
44. Wang, B.; Zhang, G.; Leng, X.; Sun, Z.; Zheng, S. Characterization and improved solar light activity of vanadium doped TiO_2 /diatomite hybrid catalysts. *J. Hazard. Mater.* **2015**, *285*, 212–220. [[CrossRef](#)]
45. Zhu, Q.; Zhang, Y.; Zhou, F.; Lv, F.; Ye, Z.; Fan, F.; Chu, P.K. Preparation and characterization of $\text{Cu}_2\text{O-ZnO}$ immobilized on diatomite for photocatalytic treatment of red water produced from manufacturing of TNT. *Chem. Eng. J.* **2011**, *171*, 61–68. [[CrossRef](#)]
46. Chen, Y.; Wu, Q.; Zhou, C.; Jin, Q. Facile preparation of Ce-doped TiO_2 /diatomite granular composite with enhanced photocatalytic activity. *Adv. Powder Technol.* **2018**, *29*, 106–116. [[CrossRef](#)]
47. Sharma, V.K.; McDonald, T.J.; Kim, H.; Garg, V.K. Magnetic graphene-carbon nanotube iron nanocomposites as adsorbents and antibacterial agents for water purification. *Adv. Colloid Interface* **2015**, *225*, 229–240. [[CrossRef](#)]
48. Hu, S.; Zhou, F.; Wang, L.; Zhang, J. Preparation of $\text{Cu}_2\text{O/CeO}_2$ heterojunction photocatalyst for the degradation of Acid Orange 7 under visible light irradiation. *Catal. Commun.* **2011**, *12*, 794–797. [[CrossRef](#)]
49. Liu, Y.; Zhu, Y.; Xu, J.; Bai, X.; Zong, R.; Zhu, Y. Degradation and mineralization mechanism of phenol by BiPO_4 photocatalysis assisted with H_2O_2 . *Appl. Catal. B Environ.* **2013**, *142*, 561–567. [[CrossRef](#)]
50. Liang, C.; Bruell, C.J.; Marley, M.C.; Sperry, K.L. Persulfate oxidation for in situ remediation of TCE. I. Activated by ferrous ion with and without a persulfate-thiosulfate redox couple. *Chemosphere* **2004**, *55*, 1213–1223. [[CrossRef](#)]

51. Zhao, J.; Zhang, Y.; Quan, X.; Chen, S. Enhanced oxidation of 4-chlorophenol using sulfate radicals generated from zero-valent iron and peroxydisulfate at ambient temperature. *Sep. Purif. Technol.* **2009**, *71*, 302–307. [[CrossRef](#)]
52. Figueroa, R.A.; Leonard, A.; MacKay, A.A. Modeling Tetracycline Antibiotic Sorption to Clays. *Environ. Sci. Technol.* **2004**, *38*, 476–483. [[CrossRef](#)] [[PubMed](#)]
53. Chu, W.; Li, D.; Gao, N.; Templeton, M.R.; Tan, C.; Gao, Y. The control of emerging haloacetamide DBP precursors with UV/persulfate treatment. *Water Res.* **2015**, *72*, 340–348. [[CrossRef](#)] [[PubMed](#)]
54. Qu, J.; Tian, X.; Jiang, Z.; Cao, B.; Akindolie, M.S.; Hu, Q.; Feng, C.; Feng, Y.; Meng, X.; Zhang, Y. Multi-component adsorption of Pb(II), Cd(II) and Ni(II) onto microwave-functionalized cellulose: Kinetics, isotherms, thermodynamics, mechanisms and application for electroplating wastewater purification. *J. Hazard. Mater.* **2020**, *387*, 121718. [[CrossRef](#)]

Sample Availability: Samples of the compounds Fe-Ce/DIA, Fe-DIA, Ce-DIA are available from the authors.

Publisher's Note: MDPI stays neutral with regard to jurisdictional claims in published maps and institutional affiliations.



© 2020 by the authors. Licensee MDPI, Basel, Switzerland. This article is an open access article distributed under the terms and conditions of the Creative Commons Attribution (CC BY) license (<http://creativecommons.org/licenses/by/4.0/>).